

Functional MR Imaging of Prostate Cancer¹

TEACHING POINTS

See last page

*Young Jun Choi, MD • Jeong Kon Kim, MD • Namkug Kim, MS
Kyoung Won Kim, MD • Eugene K. Choi, BA • Kyoung-Sik Cho, MD*

T2-weighted magnetic resonance (MR) imaging has been widely used for pretreatment work-up for prostate cancer, but its accuracy for the detection and localization of prostate cancer is unsatisfactory. To improve the utility of MR imaging for diagnostic evaluation, various other techniques may be used. Dynamic contrast material-enhanced MR imaging allows an assessment of parameters that are useful for differentiating cancer from normal tissue. The advantages of this technique include the direct depiction of tumor vascularity and, possibly, obviation of an endorectal coil; however, there also are disadvantages, such as limited visibility of cancer in the transitional zone. Diffusion-weighted imaging demonstrates the restriction of diffusion and the reduction of apparent diffusion coefficient values in cancerous tissue. This technique allows short acquisition time and provides high contrast resolution between cancer and normal tissue, but individual variability in apparent diffusion coefficient values may erode diagnostic performance. The accuracy of MR spectroscopy, which depicts a higher ratio of choline and creatine to citrate in cancerous tissue than in normal tissue, is generally accepted. The technique also allows detection of prostate cancer in the transitional zone. However, it requires a long acquisition time, does not directly depict the periprostatic area, and frequently is affected by artifacts. Thus, a comprehensive evaluation in which both functional and anatomic MR imaging techniques are used with an understanding of their particular advantages and disadvantages may help improve the accuracy of MR for detection and localization of prostate cancer.

©RSNA, 2007

Abbreviation: ADC = apparent diffusion coefficient

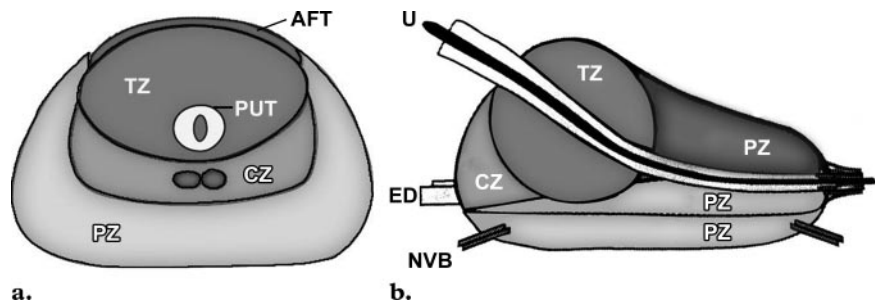
RadioGraphics 2007; 27:63–77 • Published online 10.1148/rg.271065078 • Content Codes: **GU** **MR** **01**

¹From the Department of Radiology, Research Institute of Radiology, Asan Medical Center, University of Ulsan College of Medicine, 388–1 Poongnap-dong, Songpa-gu, Seoul 138–736, South Korea (Y.J.C., J.K.K., N.K., K.W.K., K.S.C.); and Department of Radiology, Weill Medical College of Cornell University, New York, NY (E.K.C.). Recipient of a Certificate of Merit award for an education exhibit at the 2005 RSNA Annual Meeting. Received April 24, 2006; revision requested May 30 and received July 25; accepted July 26. Supported by Korean Research Foundation Grant KRF-2005–041-E00300. All authors have no financial relationships to disclose. **Address correspondence to J.K.K.** (e-mail: rialto@amc.seoul.kr).

See also the commentary by Kawashima and King following this article.

©RSNA, 2007

Figure 1. Schematics show the anatomy of the prostate in transverse (a) and sagittal (b) planes. *AFT* = anterior fibromuscular tissue, *CZ* = central zone, *ED* = ejaculatory duct, *NVB* = neurovascular bundle, *PUT* = periurethral tissue, *PZ* = peripheral zone, *U* = urethra, *TZ* = transitional zone.



Introduction

Prostate cancer is one of the most common malignancies in elderly men. In 2005, more than 232,090 Americans were diagnosed with prostate cancer and more than 30,350 died of the disease (1). In the United States, the lifetime probability of developing prostate cancer is one in six (2).

Most prostate cancers grow slowly (3,4), and early detection can lead to a complete cure. However, in more than 85% of cases of prostate cancer, multiple cancer foci are found in the prostate (5). The diagnosis of prostate cancer is based mostly on the results of ultrasonography (US)-guided transrectal biopsy. Because of the low accuracy of US for prostate cancer detection and localization, a random biopsy is usually performed instead of a targeted biopsy. However, a random biopsy has several disadvantages. For example, it may lead to an increase in complications because of the unnecessary sampling of normal prostate tissue. Moreover, cancer located outside the routine biopsy site may be missed. In addition, there may be difficulty in determining the site of a previous biopsy when repeating biopsy in a patient with a previous negative result and continuously high prostate-specific antigen levels. For these reasons, an imaging modality is needed that allows the accurate detection and localization of prostate cancer, as well as local staging, guidance of biopsy, and adequate follow-up after treatment with intensity-modulated radiation, cryosurgery, or ablation with high-intensity focused ultrasound.

Although T2-weighted MR imaging has been used widely for the pretreatment work-up of prostate cancer, the technique is limited by unsatisfactory sensitivity and specificity for cancer detection and localization. To improve the diagnostic performance of MR imaging in evaluations for prostate cancer, various other techniques have been applied. These include dynamic contrast material-enhanced MR imaging, diffusion-weighted imaging, and MR spectroscopy. The article describes the advantages and disadvantages of each of these techniques for prostate cancer detection and localization.

Anatomy of the Prostate

Approximately 70% of the prostate is composed of glandular tissue, and 30% consists of nonglandular tissue. For anatomic division of the prostate, the zonal compartment system developed by McNeal is widely accepted (6–9). According to this system, glandular tissue is subdivided into the central and the peripheral gland. The central gland is composed of a transitional zone and periurethral tissue, and the peripheral gland is composed of peripheral and central zones (Fig 1). The peripheral zone includes the posterior and lateral aspects of the prostate and accounts for most of the glandular tissue (70%). It is the zone in which 70% of prostate cancers arise. The transitional zone accounts for 5% to 10% of the glandular tissue of the prostate. Cellular proliferation in the transitional zone results in benign prostatic hyperplasia. In addition, 20% of prostate cancers arise in the transitional zone.

Conventional MR Imaging

Fast spin-echo imaging with endorectal and pelvic phased-array coils is widely used for prostate cancer evaluations (10–13). T2-weighted fast spin-echo imaging is optimal for depicting the anatomy of the prostate. Because the prostate has uniform intermediate signal intensity at T1-weighted imaging, the zonal anatomy cannot be clearly identified on T1-weighted images. On T2-weighted images, the peripheral zone has high signal intensity, in contrast to the low signal intensity of the central and transitional zones, which consist of compactly arranged smooth muscle and loose glandular tissue (Fig 2). The anterior fibromuscular stroma also has low signal intensity on T2-weighted images. The generally established protocol for T2-weighted imaging at our institution is as follows: repetition time msec/echo time msec, 4300/90; echo train length, 15; flip angle, 170°; field of view, 160–200 mm; matrix size, 768 × 768; section thickness, 4 mm; and inter-section gap, 0 mm.

On T2-weighted images, prostate cancer in the peripheral zone appears as an area of low signal intensity that is easily differentiated from high-signal-intensity normal tissue (Fig 3). However,

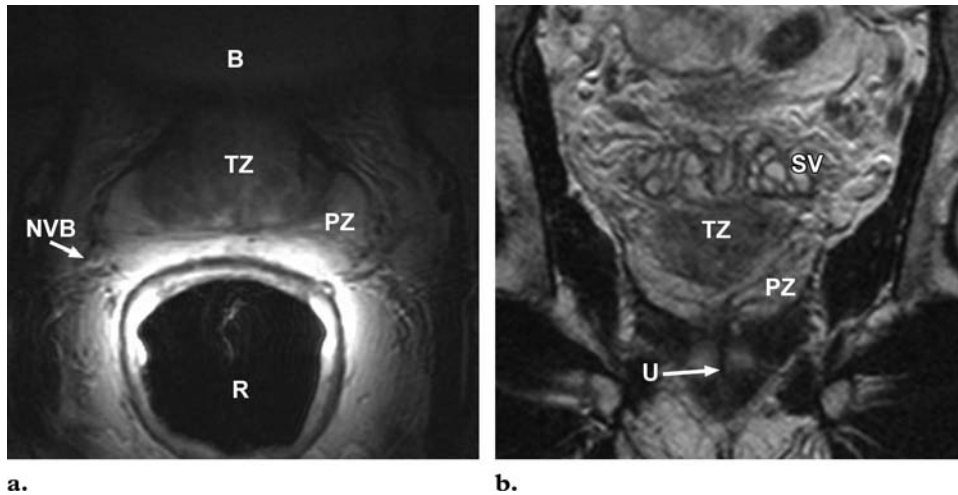


Figure 2. Axial (a) and coronal (b) T2-weighted MR images show normal zonal anatomy of the prostate. *B* = urinary bladder, *NVB* = neurovascular bundle, *PZ* = peripheral zone, *R* = rectum, *SV* = seminal vesicle, *U* = urethra, *TZ* = transitional zone.

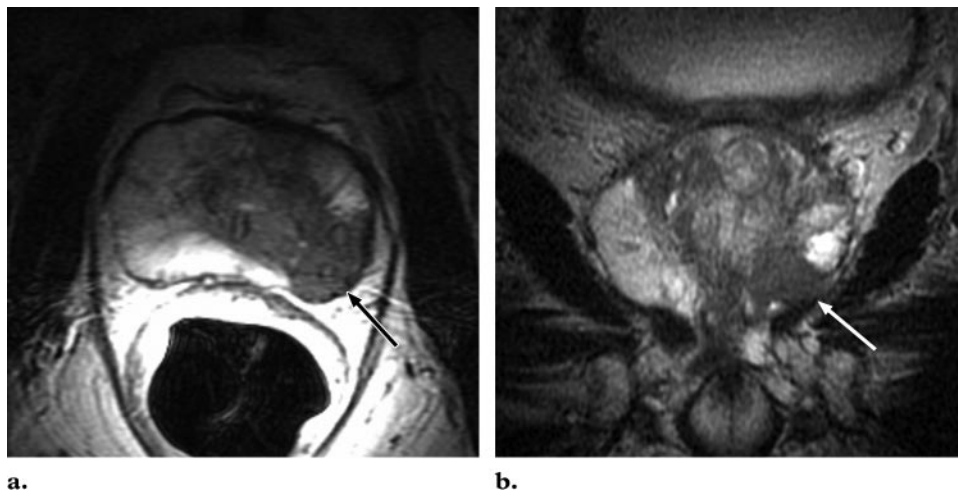


Figure 3. Biopsy-proved adenocarcinoma in a 64-year-old man. Axial (a) and coronal (b) T2-weighted MR images show an area of low signal intensity in the base of the left peripheral zone (arrow), a finding indicative of a tumor.

Teaching Point

T2-weighted imaging has significant limitations for depicting cancer in the transitional and central zones, because cancer and normal tissues both have low signal intensity on T2-weighted images. In addition, low signal intensity may be seen in the peripheral zone on T2-weighted images in the presence of many noncancerous abnormal conditions, such as nonspecific inflammation, biopsy-related hemorrhage, post-radiation therapy fibrosis, and changes after hormone deprivation therapy. Because of the anticoagulant effect of abundant citrate in normal tissue in the peripheral zone, blood products may persist 4–6 weeks or longer after prostate biopsy, leading to low signal intensity on T2-weighted images (14). Although the presence of blood products may be indicated by areas of high signal intensity on T1-weighted images, it is difficult to determine whether that finding represents cancerous tissue or only hemorrhage.

The sensitivity and specificity of T2-weighted MR imaging for prostate cancer detection have varied widely. Sensitivity of 77%–91% and specificity of 27%–61% were reported for prostate

cancer detection with T2-weighted imaging performed with an endorectal coil (15,16). Most of the previously reported data about prostate cancer detection pertain to cancer in the peripheral zone. According to the results of a study of T2-weighted imaging performed without the use of an endorectal coil, sensitivity and specificity for cancer detection were 45% and 73%, respectively (17).

Dynamic Contrast-enhanced MR Imaging

The theoretic underpinnings of this technique are based on tumor angiogenesis. In cancer, genetic mutation leads to the production and release of angiogenic factors such as the vascular permeability factor or vascular endothelial growth factor. As a result, the number of vessels increases in cancerous tissue, and the tumor vessels have greater permeability than do normal vessels, because of

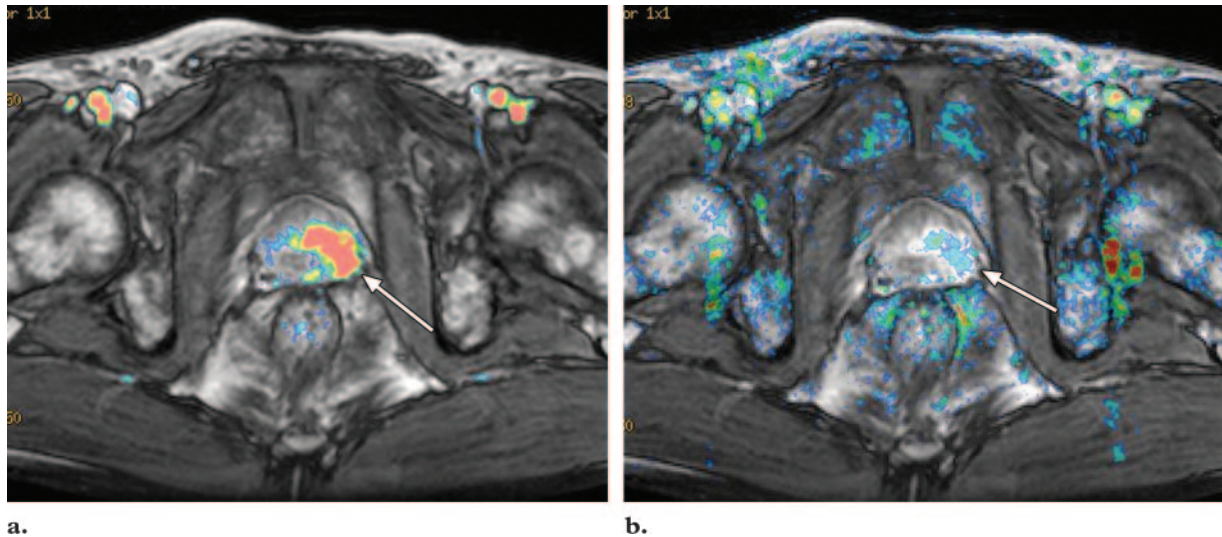
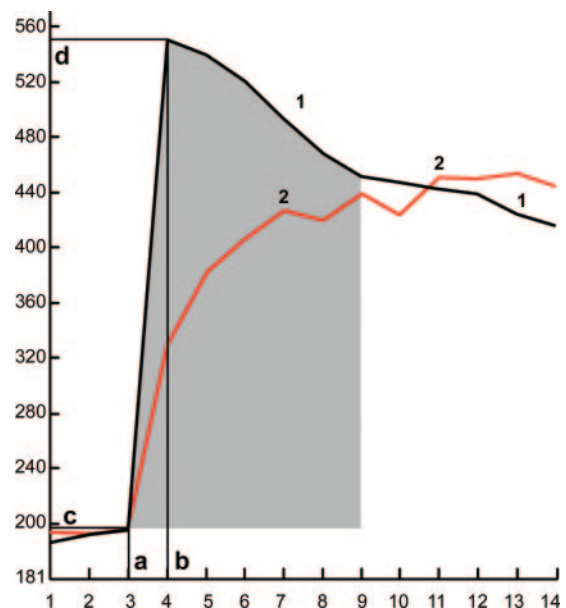


Figure 4. Biopsy-proved adenocarcinoma in a 61-year-old man. **(a)** Wash-in MR image obtained with a fast field echo sequence (17/2.9; flip angle, 20°) shows a higher wash-in rate in the right peripheral zone (arrow) than in other areas. **(b)** Washout MR image obtained with the same sequence as **a** shows a higher washout rate in the right peripheral zone (arrow) than in other areas.

Figure 5. Time-signal intensity curves from dynamic contrast-enhanced MR imaging show faster and stronger enhancement and faster washout in prostate cancer (1) than in normal tissue (red curve, 2). The x-axis shows the number of series in MR imaging, and the y-axis shows the signal intensity in arbitrary units. The onset time (*a*) is the time at which signal intensity began to increase. The time to peak (*b*) is the period between the onset time and peak enhancement. The wash-in rate (*c*) represents the velocity of enhancement and is defined by $d - c/b - a$, where *d* represents the maximum (peak) enhancement, which is defined as the absolute maximum value of enhancement. Maximum (peak) relative enhancement is defined as the difference between the absolute maximum value of enhancement and the baseline signal intensity. The washout rate is defined as the velocity of enhancement loss. The shaded area represents the area under the time-signal intensity curve for prostate cancer.



weak integrity of the vessel wall (18–20). Furthermore, because the amount of interstitial space is greater in cancerous tissue than in normal tissue, there is a larger gap of contrast material concentration between the plasma and the interstitial tissue. This characteristic environment makes the enhancement pattern of cancerous tissue different from that of normal tissue (21,22). In many experimental studies, it has been shown that the values of contrast enhancement parameters such as mean transit time, blood flow, permeability surface area, and interstitial volume are significantly greater in cancerous tissue than in normal tissue (23–27). This general observation is also applicable to prostate cancer.

With a fast imaging technique such as a gradient-echo sequence, the entire volume of the pros-

tate can be imaged in a few seconds. Although a standard MR imaging protocol for dynamic contrast-enhanced MR imaging has not been completely established, there are generally accepted requirements, such as a fast imaging sequence, minimal artifacts, and high contrast resolution. At our institution, dynamic MR imaging is performed by applying a three-dimensional fast field echo sequence (17/2.9; flip angle, 20°; section thickness, 4 mm; no intersection gap; field of view, 225 mm; matrix size, 256 × 192; 25 sections) in the axial plane. From the resultant imaging data, various perfusion parameters can be extracted according to the time sequence and analyzed to allow the detection and localization of prostate cancer (Figs 4, 5) (28–30).

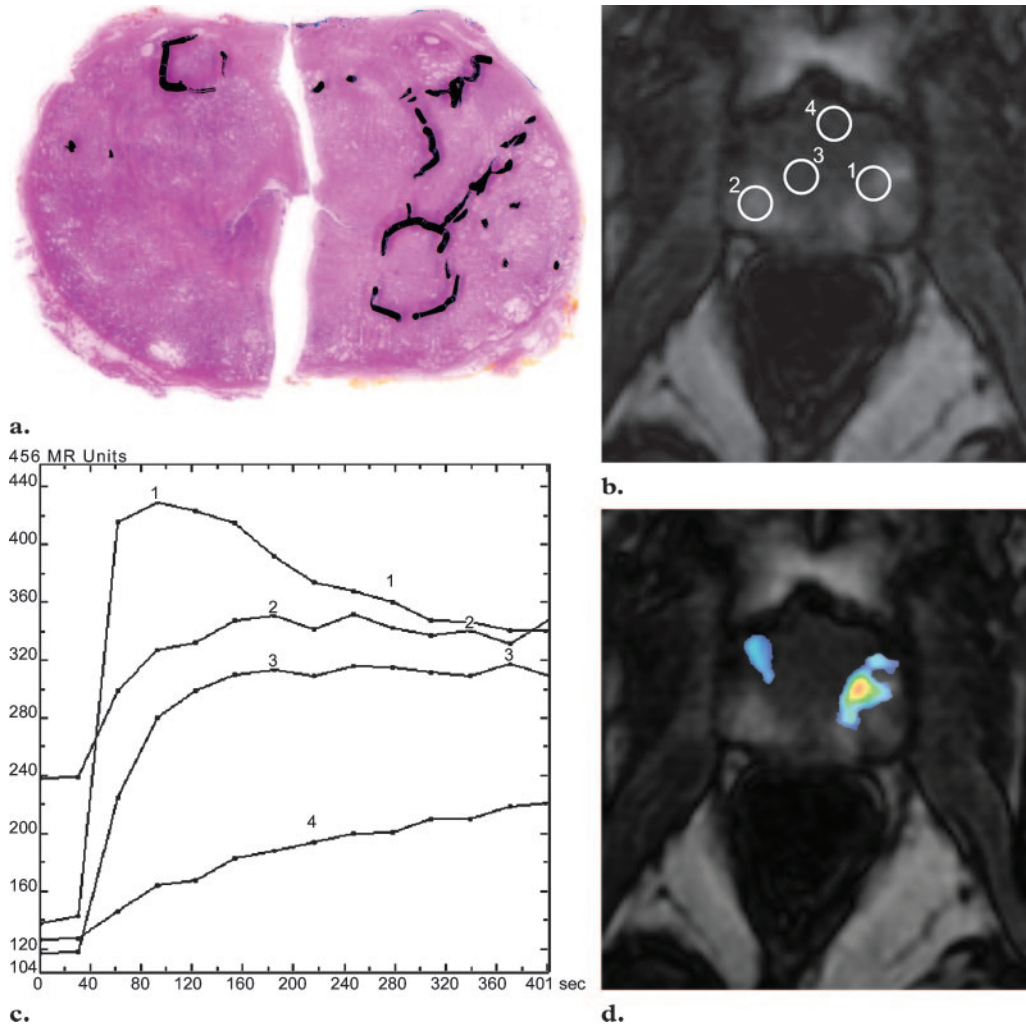
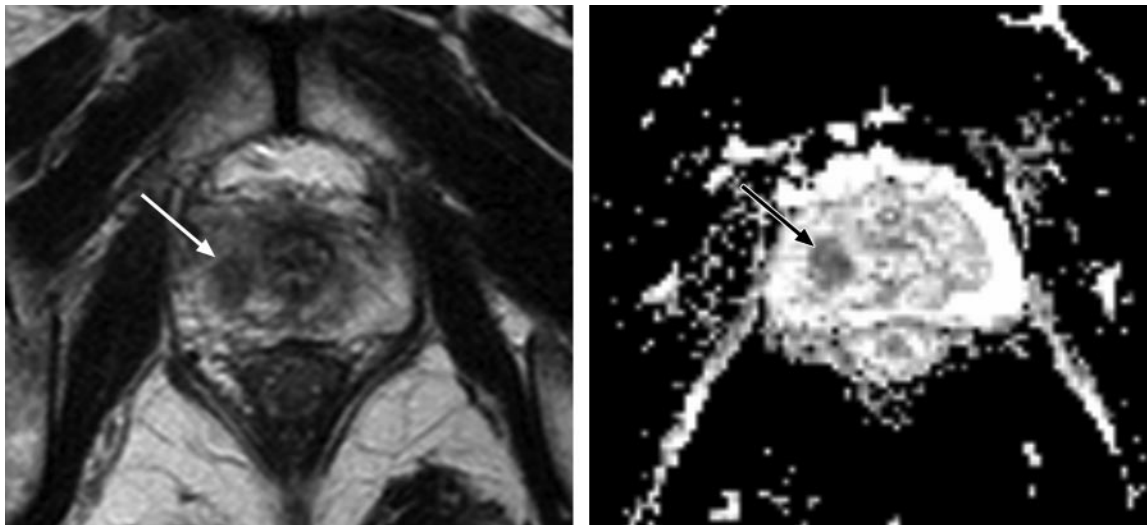


Figure 6. Parametric imaging of the wash-in rate allows detection and localization of prostate cancer in a 65-year-old man. **(a)** Histologic step section (original magnification, $\times 1$; hematoxylin-eosin stain) at the middle level of the prostate gland shows cancerous tissue (black lines and dots) in the lateral and medial peripheral zone in the left lobe and in the transitional zone in the right lobe. **(b)** Unenhanced T1-weighted MR image shows the placement of four regions of interest, according to the histologic findings, in cancerous tissue (1), normal tissue in the peripheral zone (2), normal tissue in the inner two-thirds of the transitional zone (3), and normal tissue in the outer one-third of the transitional zone (4). **(c)** Time-signal intensity curves for the four regions of interest in **b** (x-axis, time in seconds; y-axis, signal intensity in arbitrary units [au]) show wash-in rates of 9.7 au/sec for cancerous tissue (1), 2.1 au/sec for normal tissue in the peripheral zone (2), 4.3 au/sec for normal tissue in the inner two-thirds of the transitional zone (3), and 1.3 au/sec for normal tissue in the outer one-third of the transitional zone (4). **(d)** Parametric MR image at a level corresponding to that in **a** shows a wash-in rate of more than 5.7 au/sec, which was used as the threshold for differentiating cancerous tissue from normal tissue on the basis of an analysis of receiver operating characteristic curves. The parametric map of wash-in rates concurs with the histologic findings. (Reprinted, with permission, from reference 17.)

Engelbrecht et al (31) showed the usefulness of measurements of relative peak enhancement and washout rate for prostate cancer detection and localization. From their analysis of receiver operating characteristic curves, they concluded that the relative peak enhancement was the most accurate perfusion parameter for cancer detection in the peripheral zone and central region of the gland, for which the areas under the curve were, respectively, 0.93 and 0.82. Kim et al (17) demonstrated that parametric imaging of the wash-in

rate was more accurate for the detection of prostate cancer in the peripheral zone than was T2-weighted imaging alone (Fig 6). In their study, the sensitivity and specificity of peripheral zone cancer detection were 96% and 97% on parametric images of the wash-in rate but 75% and 53% on T2-weighted images ($P < .05$). However, they also observed significant overlap between the wash-in rate for cancer and that for normal tissue in the transitional zone.



a. **b.**
Figure 7. Biopsy-proved adenocarcinoma in a 72-year-old man. **(a)** Axial T2-weighted MR image shows a low-signal-intensity lesion in the right lobe of the prostate (arrow). **(b)** ADC map shows a low ADC value in the lesion (arrow), a finding indicative of decreased diffusion. A targeted biopsy was performed.

Some parameters, such as washout rate and tumor permeability, can be used for determining the effectiveness of hormone deprivation therapy as well as for the detection and localization of prostate cancer. The results of one study showed a marked reduction of tumor permeability and changes of washout pattern after androgen deprivation treatment (32).

Dynamic contrast-enhanced MR imaging has the advantage of providing direct depiction of tumor vascularity and may obviate the use of an endorectal coil. However, the limitations of this technique include unsatisfactory depiction of transitional zone cancer in patients with hypervascular benign prostatic hyperplasia. In addition, there is as yet no consensus with regard to the best acquisition protocol and the optimal perfusion parameter for differentiating cancer from normal tissue.

Diffusion-weighted Imaging

Diffusion is the process of thermally induced random molecular displacement, or brownian motion. The diffusion properties of tissue are related to the amount of interstitial free water and permeability. In general, cancer tends to have more re-

stricted diffusion than does normal tissue because of the high cell densities and abundance of intra- and intercellular membranes in cancer (33–37).

Diffusion-weighted images may be acquired with various techniques. At our institution, diffusion-weighted images are obtained by applying a gradient-echo echo-planar sequence (2700/96; flip angle, 90°; b values, 0 and 1000 sec/mm²) in the axial plane. For diffusion-weighted image interpretation, images obtained with a b value of 1000 sec/mm² are displayed by using the reverse mode, and apparent diffusion coefficient (ADC) maps are displayed by using the conventional mode.

In prostate cancer, normal glandular architecture is disrupted and replaced by aggregated cancer cells and fibrotic stroma. These changes inhibit the movement of water macromolecules, with resultant restriction of diffusion and reduction of ADC values in the cancer tissue (Fig 7). Despite significant differences in the mean ADC values between cancerous and normal tissues, individual variability may decrease the diagnostic accuracy of ADC measurement for prostate cancer detection and localization (38–43). According to the results of an analysis of receiver operating characteristic curves, the use of diffusion-weighted imaging in addition to T2-weighted

Teaching
Point

Teaching
Point

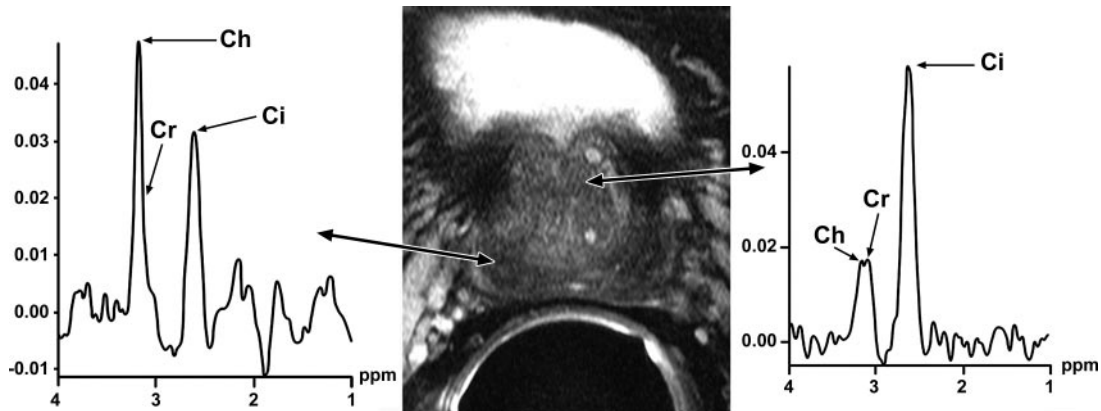


Figure 8. Biopsy-proved adenocarcinoma in a 71-year-old man. Left: MR spectrum obtained from an area of the prostate with low signal intensity at T2-weighted imaging, in which cancer was pathologically proved, demonstrates an elevated ratio (in arbitrary units) of choline (*Ch*) and creatine (*Cr*) to citrate (*Ci*). Right: MR spectrum obtained from an area with normal signal intensity shows a spectral pattern with citrate dominance and no abnormal elevation of choline and creatine.

imaging significantly improved the accuracy of tumor detection beyond that achieved with T2-weighted imaging alone (area under the curve, 0.93 for the combined imaging techniques vs 0.87 for T2-weighted imaging alone) (44).

At diffusion-weighted imaging, the diffusion sensitivity can be varied to control the image contrast. Traditionally, a b value of 1000 sec/mm² has been used because the strength of the diffusion gradients was restricted by hardware performance limitations that made it difficult to achieve acceptable echo times with higher b values. Kingsley and Monahan (45) stated that the contrast-to-noise ratio at a b value of 1000 sec/mm² is optimal for the detection of acute or chronic stroke; however, to our knowledge, there is no consensus regarding the optimal b value for prostate cancer detection. The use of higher b values may increase diffusion sensitivity by diminishing the hyperintensity of tissues with long T2 relaxation times (ie, T2 shine-through). However, high b values may lead to decreased absolute differences in signal intensity between cancer and normal tissue.

Diffusion-weighted imaging has advantages such as short acquisition time and high contrast resolution between tumors and normal tissue. However, this technique is limited by poor spatial resolution and the potential risk of image distortion caused by postbiopsy hemorrhage, which results in magnetic field inhomogeneity.

MR Spectroscopy

MR spectroscopy provides metabolic information about prostate tissue by demonstrating the relative concentration of chemical compounds. Normal prostate tissue contains a high level of citrate. In prostate cancer, the citrate level decreases as the citrate-producing metabolism of normal tissue is converted to a citrate-oxidating metabolism. At the same time, the level of choline in cancer is elevated because of a high turnover of phospholipid in cell membranes in the proliferating tissue. Consequently, the ratio of choline to citrate is increased in cancerous tissue. Because of the proximity of the choline and creatine peaks at MR spectroscopy performed with a 1.5-T MR unit, the ratio of choline and creatine to citrate, which also is increased in prostate cancer, is the parameter measured (Fig 8).

Among the various MR spectroscopic sequences, the most widely used technique is three-dimensional chemical shift imaging (46) with point-resolved spectroscopy, voxel excitation, and band-selective inversion with gradient dephasing for water and lipid suppression (47). Chemical shift imaging refers to a technique that allows the acquisition of voxels in multiple sections and the display of parametric maps (of the ratio of choline

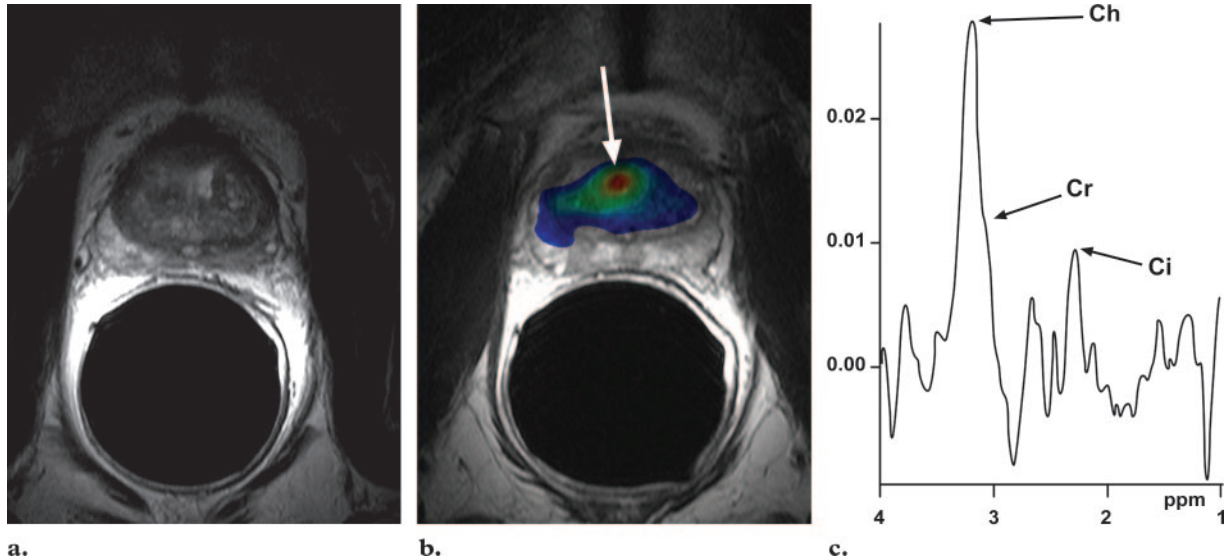


Figure 9. Biopsy-proved adenocarcinoma in a 65-year-old man with a previous negative biopsy result and a continuously elevated prostate-specific antigen level. **(a)** Axial T2-weighted MR image shows no focal lesion in the prostate. **(b, c)** MR spectroscopic image **(b)** and corresponding spectrum **(c)** demonstrate an elevated ratio (in arbitrary units) of choline (*Ch*) and creatine (*Cr*) to citrate (*Ci*) in the central gland (arrow in **b**), a finding indicative of prostate cancer, which was confirmed at targeted biopsy.

and creatine to citrate) in correlation with T2-weighted morphologic images.

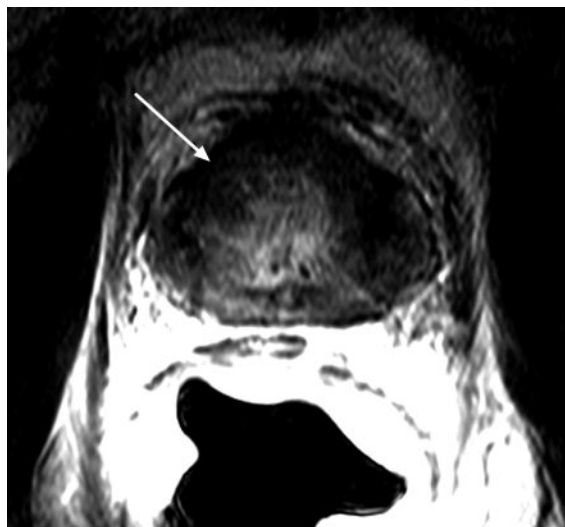
According to Kurhanewicz et al (48), peripheral-zone voxels in which the ratio of choline and creatine to citrate is at least 2 standard deviations above the average ratio are considered to represent possible cancer. Voxels are considered very suggestive of cancer if the ratio of choline and creatine to citrate is more than 3 standard deviations above the average ratio (49). However, no consensus has been reached about the metabolite ratio that can exactly determine the presence of prostate cancer, and there may be individual variability in spectral analysis among patients. Furthermore, a voxel may contain nondiagnostic levels of metabolites or may be affected by an artifact that obscures the metabolite frequency range.

The combined use of MR spectroscopy and MR imaging has been shown to improve cancer detection and localization in the peripheral zone (16) and cancer volume measurement in the peripheral zone (50). Scheidler et al (16) demonstrated a sensitivity and specificity for cancer detection of 91% and 95% for combined MR spectroscopy and MR imaging, but 77%–81% and

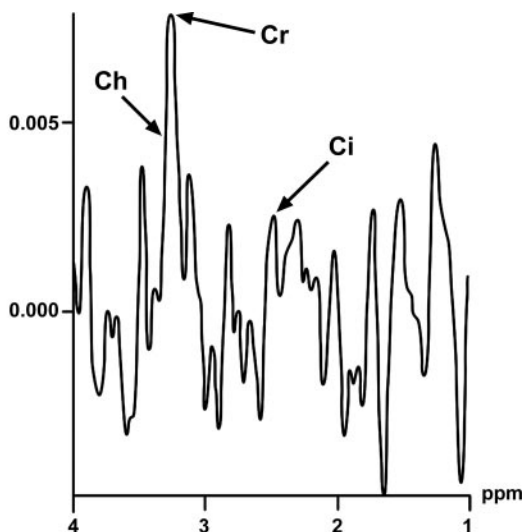
46%–61% for MR imaging alone and 63% and 75% for MR spectroscopy alone. Furthermore, on the basis of a strong correlation between the volume of prostate cancer and its extracapsular extension (51–53), investigators have shown that the combination of volumetric data from MR spectroscopy and T2-weighted imaging may result in improved accuracy in determining extracapsular tumor extension (54).

In recent years, other merits of MR spectroscopy have been noted. The results of several studies show that prostate biopsy directed with endorectal MR spectroscopy may help increase the cancer detection rate in patients with an elevated prostate-specific antigen level and a previous negative biopsy result (55) (Fig 9). In addition, investigators have observed a trend toward an increasing ratio of choline and creatine to citrate in association with an increasing Gleason score, a trend suggestive of the potential usefulness of MR spectroscopy for noninvasive estimation of cancer aggressiveness (56).

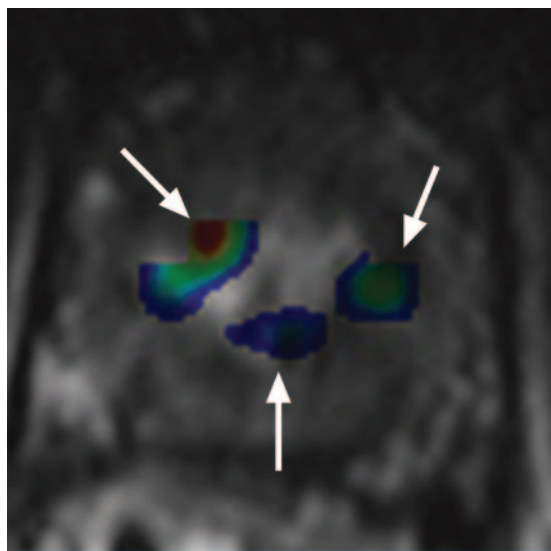
MR spectroscopy also is more useful than conventional MR imaging for detecting transitional zone cancer (Fig 10). However, the cancer metabolite ratio in the transitional zone varies broadly, and thus there may be overlap in me-



a.



b.



c.

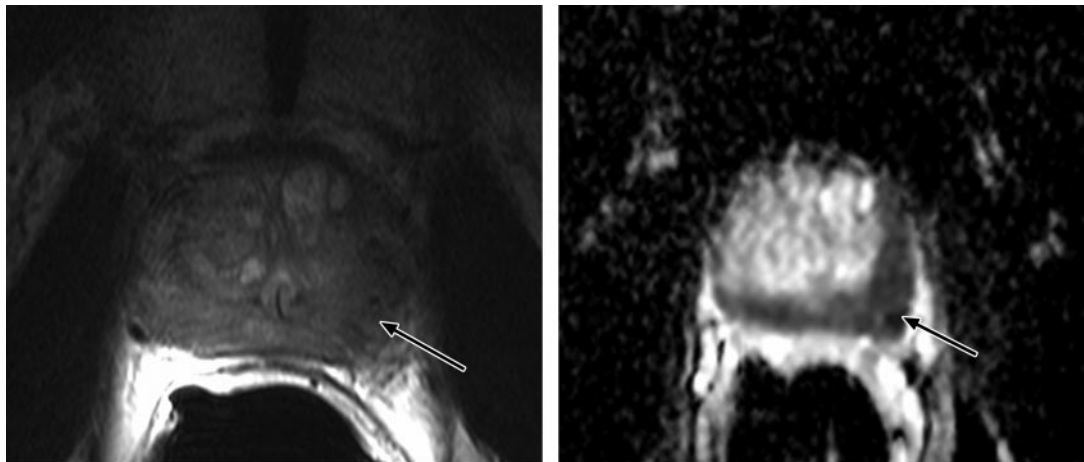
Figure 10. Biopsy-proved adenocarcinoma in the central zone in both lobes of the prostate in a 67-year-old man. **(a)** Axial T2-weighted MR image shows areas of abnormally low signal intensity (arrow), a finding that is not definitively indicative of cancer. **(b, c)** MR spectrum **(b)** and spectroscopic image **(c)** show high ratios (in arbitrary units) of choline (*Ch*) and creatine (*Cr*) to citrate (*Ci*) in three areas (arrows in **c**). The findings were indicative of cancer, which was diagnosed at targeted biopsy.

tabolite ratios between cancerous and benign tissues in the transitional zone (57).

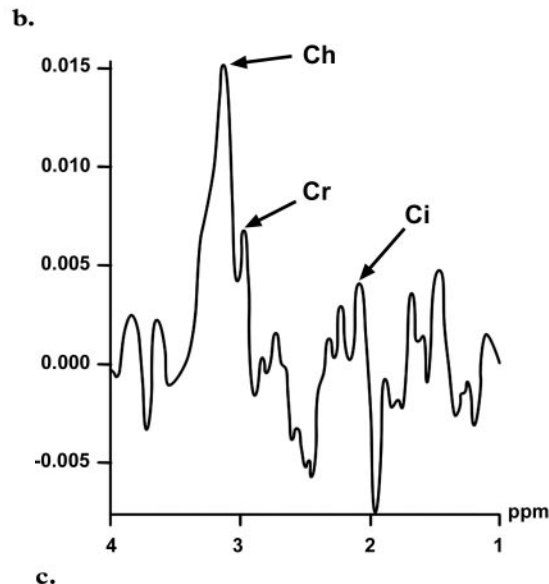
MR spectroscopy is useful, in addition, for planning treatment and determining therapeutic effectiveness, as well as for detecting a recurrent tumor after surgery, radiation therapy, or hormone deprivation therapy. The ratio of choline and creatine to citrate is indicative of the tumor response to treatment (58–61).

The advantages of MR spectroscopy are its generally accepted accuracy, its capability for depicting possible cancer in the transitional zone, and its widely proved diagnostic performance. However, the technique is disadvantaged by long acquisition time, possible variability in results dependent on postprocessing or shimming, and no direct visualization of the periprostatic anatomy.

Furthermore, a previous prostate biopsy may lead to spectral degradation that makes accurate interpretation of the metabolite ratios impossible. According to the results of a previous study, the mean percentage of degraded peripheral-zone voxels was 19% at MR spectroscopy performed within 8 weeks after biopsy, compared with 7% after 8 weeks (62). An adequate time interval is necessary between prostatic biopsy and MR examination. In another study, investigators showed that, despite the potential risk of hemorrhage, MR spectroscopy may improve the ability to determine the presence of prostate cancer and its spatial extent when postbiopsy changes hinder interpretation with the use of conventional MR images alone (63).



a.
Figure 11. Biopsy-proved adenocarcinoma in a 65-year-old man. **(a)** Axial T2-weighted MR image shows an area of low signal intensity (arrow) in the left peripheral zone of the prostate. **(b)** ADC map shows a low ADC value in the same area (arrow). **(c)** MR spectrum obtained in the abnormal area shows an elevated ratio (in arbitrary units) of choline (*Ch*) and creatine (*Cr*) to citrate (*Ci*).



Conclusions

Various MR imaging techniques beyond conventional T2-weighted imaging can provide improved cancer detection and localization, as well as information regarding the biologic behavior, volume, and staging of cancers for individualized therapy. However, each technique has one or more limitations, such as no standard parameters, or low accuracy in the central region of the gland. No randomized large study has been performed to compare the techniques, and there has been no report with regard to which technique is best in a specific clinical situation. Furthermore, the existing literature contains little information about the effectiveness of MR imaging at 3.0 T for the evaluation of prostate cancer. Therefore, a comprehensive understanding of the advantages and disadvantages of various MR imaging techniques and protocols is expected to improve the MR-based detection and localization of prostate cancer (Figs 11, 12).

References

1. Jemal A, Murray T, Ward E, et al. Cancer statistics, 2005. *CA Cancer J Clin* 2005;55:10–30.
2. Mazhar D, Waxman J. Prostate cancer. *Postgrad Med J* 2002;78:590–595.
3. Johansson JE, Holmberg L, Johansson S, Bergstrom R, Adami HO. Fifteen-year survival in prostate cancer: a prospective, population-based study in Sweden. *JAMA* 1997;277:467–471.
4. Pound CR, Partin AW, Eisenberger MA, Chan DW, Person JD, Walsh PC. Natural history of progression after PSA elevation following radical prostatectomy. *JAMA* 1999;281:1591–1597.
5. Byar DP, Mostofi FK. Carcinoma of the prostate: prognostic evaluation of certain pathologic features in 208 radical prostatectomies examined by the step-section technique. *Cancer* 1972;30:5–13.
6. Hricak H, Thoeni RF. Anatomy of the prostate gland. In: Pollack HM. *Clinical urography*. 2nd ed. Philadelphia, Pa: Saunders, 2000; 1669–1670.
7. Coakley FV, Hricak H. Radiologic anatomy of the prostate gland: a clinical approach. *Radiol Clin North Am* 2000;38:15–30.
8. Villers A, Steg A, Boccon-Gibod L. Anatomy of the prostate: review of the different models. *Eur Urol* 1991;20:261–268.
9. Hricak H, Dooks GC, McNeal JE, et al. MR imaging of the prostate gland: normal anatomy. *AJR Am J Roentgenol* 1987;148:51–58.

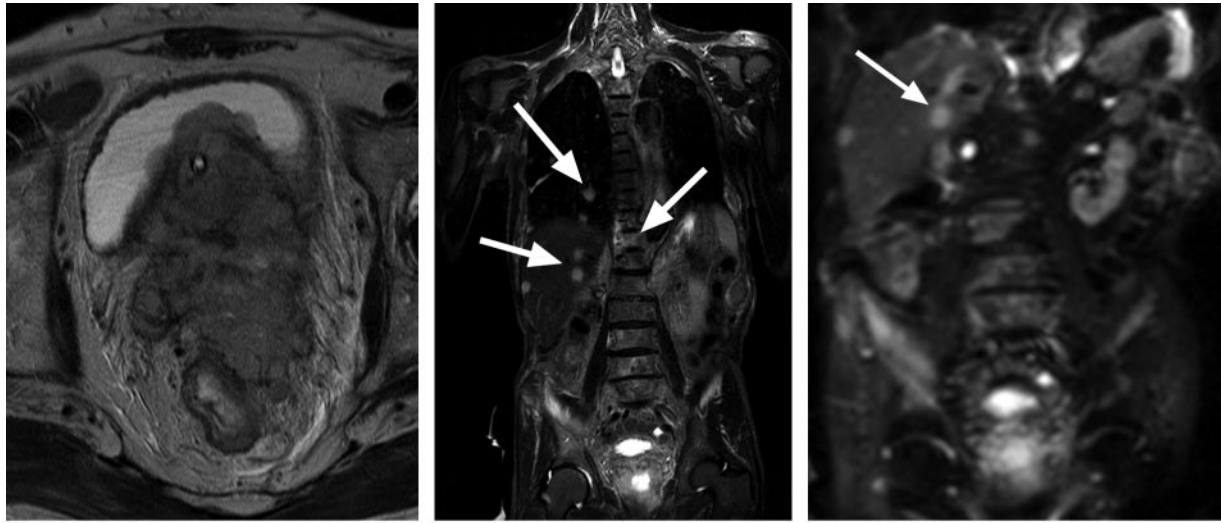


Figure 12. Biopsy-proved adenocarcinoma of the whole prostate in a 75-year-old man. **(a)** Axial T2-weighted MR image shows a huge contoured mass that involves the entire prostate and that has invaded the urinary bladder and rectum. **(b)** Coronal T2-weighted MR image of the abdomen and pelvis shows multiple metastases in the liver, lungs, and thoracolumbar spine (arrows). **(c)** Coronal diffusion-weighted image of the abdomen and pelvis shows multifocal restriction of diffusion in the liver and thoracolumbar spine (arrow).

10. Schnall MD, Lenkinski RE, Pollack HM, Imai Y, Kressel HY. Prostate: MR imaging with an endorectal surface coil. *Radiology* 1989;172:570–574.
11. Quinn SF, Franzini DA, Demlow TA, et al. MRI of prostate cancer with an endorectal surface coil technique: correlation with whole mount specimens. *Radiology* 1994;190:323–327.
12. Perrotti M, Kaufman RP Jr, Jennings TA, et al. Endo-rectal coil magnetic resonance imaging in clinically localized prostate cancer: is it accurate? *J Urol* 1996;156:106–109.
13. Claus FG, Hricak H, Hattery RR. Pretreatment evaluation of prostate cancer: role of MR imaging and ^1H MR spectroscopy. *RadioGraphics* 2004; 24(suppl 1):S167–S180.
14. White S, Hricak H, Forstner R, et al. Prostate cancer: effect of postbiopsy hemorrhage on interpretation of MR images. *Radiology* 1995;195:385–390.
15. Hricak H, White S, Vigneron D, et al. Carcinoma of the prostate gland: MR imaging with pelvic phased-array coils versus integrated endorectal-pelvic phased-array coils. *Radiology* 1994;193: 703–709.
16. Scheidler J, Hricak H, Vigneron DB, et al. Prostate cancer: localization with three-dimensional proton MR spectroscopic imaging—clinicopathologic study. *Radiology* 1999;213:473–480.
17. Kim JK, Hong SS, Choi YJ, et al. Wash-in rate on the basis of dynamic contrast-enhanced MRI: usefulness for prostate cancer detection and localization. *J Magn Reson Imaging* 2005;22:639–646.
18. Weidner N, Carroll PR, Flax J, Blumenfeld W, Folkman J. Tumor angiogenesis correlates with metastasis in invasive prostate carcinoma. *Am J Pathol* 1993;143:401–409.
19. Brawer MK, Deering RE, Brown M, Preston SD, Bigler SA. Predictors of pathologic stage in prostatic carcinoma: the role of neovascularity. *Cancer* 1994;73:678–687.
20. Siegal JA, Yu E, Brawer MK. Topography of neovascularity in human prostate carcinoma. *Cancer* 1995;75:2545–2551.
21. Delorme S, Knopp MV. Non-invasive vascular imaging: assessing tumour vascularity. *Eur Radiol* 1998;8:517–527.
22. Yamashita Y, Baba T, Baba Y, et al. Dynamic contrast-enhanced MR imaging of uterine cervical cancer: pharmacokinetic analysis with histopathologic correlation and its importance in predicting the outcome of radiation therapy. *Radiology* 2000; 216:803–809.
23. Buckley DL, Roberts C, Parker GJ, Logue JP, Hutchinson CE. Prostate cancer: evaluation of vascular characteristics with dynamic contrast-enhanced T1-weighted MR imaging—initial experience. *Radiology* 2004;233:709–715.
24. Brix G, Semmler W, Port R, Schad LR, Layer G, Lorenz WJ. Pharmacokinetic parameters in CNS Gd-DTPA enhanced MRI. *J Comput Assist Tomogr* 1991;15:621–628.
25. Hoffmann U, Brix G, Knopp MV, Hess T, Lorenz WJ. Pharmacokinetic mapping of the breast: a new method for dynamic MR-mammography. *Magn Reson Med* 1995;33:506–514.
26. Hawighorst H, Knopp MV, Debus J, et al. Pharmacokinetic MRI for assessment of malignant glioma response to stereotactic radiotherapy: initial results. *J Magn Reson Imaging* 1998;8:783–788.
27. Port RE, Knopp MV, Hoffmann U, Milker-Zabel S, Brix G. Multicompartment analysis of gadolinium chelate kinetics: blood-tissue exchange in mammary tumors as monitored by dynamic MR imaging. *J Magn Reson Imaging* 1999;10:233–241.

28. Liney GP, Turnbull LW, Knowles AJ. In vivo magnetic resonance spectroscopy and dynamic contrast enhanced imaging of the prostate gland. *NMR Biomed* 1999;12:39–44.
29. Turnbull LW, Buckley DL, Turnbull LS, Liney GP, Knowles AJ. Differentiation of prostatic carcinoma and benign prostatic hyperplasia: correlation between dynamic Gd-DTPA-enhanced MRI and histopathology. *J Magn Reson Imaging* 1999;9:311–316.
30. Rouviere O, Raudrant A, Ecochard R, et al. Characterization of time-enhancement curves of benign and malignant prostate tissue at dynamic MRI. *Eur Radiol* 2003;13:931–942.
31. Engelbrecht MR, Huisman HJ, Laheij RJ, et al. Discrimination of prostate cancer from normal peripheral zone and central gland tissue by using dynamic contrast-enhanced MR imaging. *Radiology* 2003;229:248–254.
32. Padhani AR, MacVicar AD, Gapinski CJ, et al. Effects of androgen deprivation on prostatic morphology and vascular permeability evaluated with MR imaging. *Radiology* 2001;218:365–374.
33. Tien RD, Felsberg GJ, Friedman H, Brown M, MacFall J. MR imaging of high-grade cerebral gliomas: value of diffusion-weighted echoplanar pulse sequences. *AJR Am J Roentgenol* 1994;162:671–677.
34. Eis M, Els T, Hoehn-Berlage M, Hossmann KA. Quantitative diffusion MR imaging of cerebral tumor and edema. *Acta Neurochir Suppl (Wien)* 1994;60:344–346.
35. Eis M, Els T, Hoehn-Berlage M. High resolution quantitative relaxation and diffusion MRI of three different experimental tumors in rat. *Magn Reson Med* 1995;34:835–844.
36. Sugahara T, Korogi Y, Kochi M, et al. Usefulness of diffusion-weighted MRI with echo-planar technique in the evaluation of cellularity in gliomas. *J Magn Reson Imaging* 1999;9:53–60.
37. Castillo M, Smith JK, Kwock L, Wilber K. Apparent diffusion coefficients in the evaluation of high-grade cerebral gliomas. *AJNR Am J Neuroradiol* 2001;22:60–64.
38. Sato C, Naganawa S, Nakamura T, et al. Differentiation of noncancerous tissue and cancer lesions by apparent diffusion coefficient values in transition and peripheral zones of the prostate. *J Magn Reson Imaging* 2005;21:258–262.
39. Issa B. In vivo measurement of the apparent diffusion coefficient in normal and malignant prostatic tissues using echo-planar imaging. *J Magn Reson Imaging* 2002;16:196–200.
40. Hosseinzadeh K, Schwarz SD. Endorectal diffusion-weighted imaging in prostate cancer to differentiate malignant and benign peripheral zone tissue. *J Magn Reson Imaging* 2004;20:654–661.
41. Gibbs P, Tozer DJ, Liney GP, Turnbull LW. Comparison of quantitative T2 mapping and diffusion-weighted imaging in the normal and pathologic prostate. *Magn Reson Med* 2001;46:1054–1058.
42. Chan I, Wells W 3rd, Mulkern RV, et al. Detection of prostate cancer by integration of line-scan diffusion, T2-mapping and T2-weighted magnetic resonance imaging; a multichannel statistical classifier. *Med Phys* 2003;30:2390–2398.
43. Scheidler J, Petsch R, Mueller-Lisse U, Heuck AF, Reiser M. Echo-planar diffusion-weighted MR imaging of the prostate [abstr]. In: *Proceedings of the Seventh Meeting of the International Society for Magnetic Resonance in Medicine*. Berkeley, Calif: International Society for Magnetic Resonance in Medicine, 1999; 1103.
44. Shimofusa R, Fujimoto H, Akamata H, et al. Diffusion-weighted imaging of prostate cancer. *J Comput Assist Tomogr* 2005;29:149–153.
45. Kingsley PB, Monahan WG. Selection of the optimum b factor for diffusion-weighted magnetic resonance imaging assessment of ischemic stroke. *Magn Reson Med* 2004;51:996–1001.
46. Brown TR, Kincaid BM, Ugurbil K. NMR chemical shift imaging in three dimensions. *Proc Natl Acad Sci U S A* 1982;79:3523–3526.
47. Star-Lack J, Nelson SJ, Kurhanewicz J, Huang LR, Vigneron DB. Improved water and lipid suppression for 3D PRESS CSI using RF band-selective inversion with gradient dephasing (BASING). *Magn Reson Med* 1997;38:311–321.
48. Kurhanewicz J, Vigneron DB, Hricak H, Narayan P, Carroll P, Nelson SJ. Three-dimensional H-1 spectroscopic imaging of the in situ human prostate with high (0.24–0.7-cm³) spatial resolution. *Radiology* 1996;198:795–805.
49. Males RG, Vigneron DB, Star-Lack J, et al. Clinical application of BASING and spectral/spatial water and lipid suppression pulses for prostate cancer staging and localization by in vivo 3D 1H magnetic resonance spectroscopic imaging. *Magn Reson Med* 2000;43:17–22.
50. Coakley FV, Kurhanewicz F, Lu Y, et al. Prostate cancer tumor volume: measurement with endorectal MR and MR spectroscopic imaging. *Radiology* 2002;223:91–97.
51. Stamey TA, McNeal JE, Freiha FS, Redwine E. Morphometric and clinical studies on 68 consecutive radical prostatectomies. *J Urol* 1988;139:1235–1241.
52. Bostwick DG, Graham SD Jr, Napalkov P, et al. Staging of early prostate cancer: a proposed tumor volume-based prognostic index. *Urology* 1993;41:403–411.
53. McNeal JE, Villers AA, Redwine EA, Freiha FS, Stamey TA. Capsular penetration in prostate cancer: significance for natural history and treatment. *Am J Surg Pathol* 1990;14:240–247.
54. Yu KK, Scheidler J, Hricak H, et al. Prostate cancer: prediction of extracapsular extension with endorectal MR imaging and three-dimensional proton MR spectroscopic imaging. *Radiology* 1999;213:481–488.
55. Prando A, Kurhanewicz J, Borges AP, Oliveira EM Jr, Figueiredo E. Prostatic biopsy directed with endorectal MR spectroscopic imaging findings in patients with elevated prostate specific anti-

- gen levels and prior negative biopsy findings: early experience. *Radiology* 2005;236:903–910.
56. Zakian KL, Sircar K, Hricak H, et al. Correlation of proton MR spectroscopic imaging with Gleason score based on step-section pathologic analysis after radical prostatectomy. *Radiology* 2005;234:804–814.
 57. Zakian KL, Eberhardt S, Hricak H, et al. Transition zone prostate cancer: metabolic characteristics at ¹H MR spectroscopic imaging—initial results. *Radiology* 2003;229:241–247.
 58. Pucar D, Shukla-Dave A, Hricak H, et al. Prostate cancer: correlation of MR imaging and MR spectroscopy with pathologic findings after radiation therapy—initial experience. *Radiology* 2005;236:545–553.
 59. Mueller-Lisse UG, Vigneron DB, Hricak H, et al. Localized prostate cancer: effect of hormone deprivation therapy measured by using combined three-dimensional ¹H MR spectroscopy and MR imaging: clinicopathologic case-controlled study. *Radiology* 2001;221:380–390.
 60. Wang L, Mullerad M, Chen HN, et al. Prostate cancer: incremental value of endorectal MR imaging findings for prediction of extracapsular extension. *Radiology* 2004;232:133–139.
 61. Coakley FV, Teh HS, Qayyum A, et al. Endorectal MR imaging and MR spectroscopic imaging for locally recurrent prostate cancer after external beam radiation therapy: preliminary experience. *Radiology* 2004;233:441–448.
 62. Qayyum A, Coakley FV, Lu Y, et al. Organ-confined prostate cancer: effect of prior transrectal biopsy on endorectal MRI and MR spectroscopic imaging. *AJR Am J Roentgenol* 2004;183:1079–1083.
 63. Kaji Y, Kurhanewicz J, Hricak H, et al. Localizing prostate cancer in the presence of postbiopsy change on MR images: role of proton MR spectroscopic imaging. *Radiology* 1998;206:785–790.

Functional MR Imaging of Prostate Cancer

Young Jun Choi, MD et al

RadioGraphics 2007; 27:63-77 • Published online 10.1148/rg.271065078 • Content Codes: **GU** **MR** **O1**

Page 65

T2-weighted imaging has significant limitations for depicting cancer in the transitional and central zones, because cancer and normal tissues both have low signal intensity on T2-weighted images. In addition, low signal intensity may be seen in the peripheral zone on T2-weighted images in the presence of many noncancerous abnormal conditions.

Page 68

Dynamic contrast-enhanced MR imaging has the advantage of providing direct depiction of tumor vascularity and may obviate the use of an endorectal coil. However, the limitations of this technique include unsatisfactory depiction of transitional zone cancer in patients with hypervascular benign prostatic hyperplasia. In addition, there is as yet no consensus with regard to the best acquisition protocol and the optimal perfusion parameter for differentiating cancer from normal tissue.

Page 68

Despite significant differences in the mean ADC values between cancerous and normal tissues, individual variability may decrease the diagnostic accuracy of ADC measurement for prostate cancer detection and localization.

Page 71

The advantages of MR spectroscopy are its generally accepted accuracy, its capability for depicting possible cancer in the transitional zone, and its widely proved diagnostic performance. However, the technique is disadvantaged by long acquisition time, possible variability in results dependent on postprocessing or shimming, and no direct visualization of the periprostatic anatomy.

Page 72

Various MR imaging techniques beyond conventional T2-weighted imaging can provide improved cancer detection and localization, as well as information regarding the biologic behavior, volume, and staging of cancers for individualized therapy. However, each technique has one or more limitations, such as no standard parameters, or low accuracy in the central region of the gland. No randomized large study has been performed to compare the techniques, and there has been no report with regard to which technique is best in a specific clinical situation.